This article has been accepted for publication in a future issue of this journal, but has not been fully edited. Content may change prior to final publication. Citation information: DOI 10.1109/ACCESS.2020.2993361, IEEE Access

IEEE Access
Multidisciplinary | Rapid Review | Open Access Journal

Date of publication xxxx 00, 0000, date of current version xxxx 00, 0000.

Digital Object Identifier 10.1109/ACCESS.2017.DOI

An Improved Bat Algorithm for More Efficient and Faster Maximum Power Point Tracking for a Photovoltaic System Under Partial Shading Conditions

CHIH YU LIAO[1], RAMADHANI KURNIAWAN SUBROTO[2], (MEMBER, IEEE), IBRAHIM SAIFUL MILLAH[3], KUO LUNG LIAN[4], (SENIOR MEMBER, IEEE), AND WEI-TZER HUANG[5], (MEMBER, IEEE)

[1,2,3,4]Department of Electrical Engineering, National Taiwan University of Science and Technology, Taipei, Taiwan, 106, R.O.C. (e-mail: ryanlian@gapps.ntust.edu.tw)
[5]Department of Industrial Education and Technology, National Changhua University of Education

Corresponding author: Kuo Lung Lian (e-mail: ryanlian@gapps.ntust.edu.tw).

ABSTRACT Solar modules under partial shading (PS) conditions will result in power and voltage characteristic curves (P-VCC) having multiple peaks. If the maximum power point cannot be obtained, the output power of the solar modules will be greatly reduced. Hence, there have been various maximum power point tracking (MPPT) control methods developed to address this problem. One alternative is to employ the meta-heuristic approach (MHA) to track the global maximum power point (GMPP). Recently, a new MHA called Bat Algorithm (BA) has performed well in the MPPT. Nevertheless, BA may fail to track the GMPP when there are some local maximum power points (LMPPs) close to the GMPP. Also, the tracking time needs to be further reduced to accommodate rapidly changing irradiance. Therefore, a combination of BA with the abandonment mechanism of Cuckoo Search (CS) is proposed to improve the tracking performance of the BA. Both simulation and experimental results show that the proposed method, as compared to BA, yields better accuracy and an improvement of convergence speed of about 35% for various P-VCCs can be achieved. Moreover, the MBA has also been tested against some of the state-of-the-art MPPT algorithms such as Particle Swarm Optimization and Grey Wolf Optimization (GWO), and the results showed the superiority of the proposed method.

INDEX TERMS Bat algorithm, Cuckoo Search, Maximum Power Point Tracking, Partial shading

I. INTRODUCTION

IN recent years, the rise of environmental awareness and the greenhouse effect have led many countries to actively develop renewable energy sources such as solar, wind, tidal and geothermal energies. According to the market forecast of the International Energy Agency (IEA), the renewable energy will account for nearly one-third of world's total power generation by 2023, and solar energy will grow the most [1]. Therefore, it has become the main force of renewable energy development [2], [3]. The IEA report shows that the solar energy growth rate of the world is about 31.2% in 2017 - 2018. This number is larger than those of the wind power (12.2%) and hydro-power (3.1%) combined [4].

Photovoltaic power generation systems convert solar energy into electrical energy [5]–[8]. The voltage-current relationship of a single photovoltaic (PV) module exhibits a nonlinear relationship, thus creating a set of maximum power points that vary depending on irradiance and temperature. In practical applications, the PV modules are connected in series. When some of these modules are partially shaded due to cloud, buildings, and etc, they will limit the current and voltage of the entire PV panel, which drastically reduces the system efficiency [9], [10].

Partial shading (PS) will cause hot spots in shaded areas, leading to acceleration of component aging. In order to reduce their impacts, one common solution is to add bypass diodes between each PV module [11], [12]. However, this method will cause the overall P-V characteristic curve (P-

This work is licensed under a Creative Commons Attribution 4.0 License. For more information, see https://creativecommons.org/licenses/by/4.0/.

This article has been accepted for publication in a future issue of this journal, but has not been fully edited. Content may change prior to final publication. Citation information: DOI 10.1109/ACCESS.2020.2993361, IEEE Access

VCC) to exhibit multiple peaks [13], [14]. Therefore, the aim of a maximum power point tracking (MPPT) controller is to extract the global maximum power point (GMPP) under various conditions (with or without PS) [15], [16]. One common approach is to track the GMPP by developing advanced control algorithm (ACA), classified into deterministic-based MPPT and artificial intelligence-based (AI) MPPT.

The common algorithms used in industrial applications, such as perturb and observe (P&O) [17]–[19], hill climbing (HC) [20], and incremental conductance (InC) [21], [22], fall into deterministic-based MPPT category. P&O has the advantage of easy implementation and fast tracking. However, it tends to oscillate around the maximum power point and cannot be ensured to obtain the GMPP under PS. If the perturbation size is not wisely chosen, the oscillation can easily occur. Many attempts have been made to reduce the oscillation around the maximum power point (MPP) [18], [23]. Changing the fixed step size into adaptive one is one way to improve the P&O as introduced in [17]–[19], [24]. For instance, [24] proposed an adaptive P&O based on the derivative of power with respect to voltage to have faster dynamics and improved stability compared to the traditional P&O method. Moreover, the trigonometry rule is combined with InC method to reduce the convergence time for achieving GMPP [25]. Nevertheless, these improved methods still cannot attain the GMPP of P-VCCs with multiple peaks.

AI-based MPPT is a promising approach to achieve GMPP for P-VCC with multiple peaks. AI-based MPPT can be categorized into fuzzy logic (FL) [26]–[28], artificial neural network (ANN) [29]–[31], and meta-heuristic approaches (MHAs) [32]–[34]. In [35], the FL method combined with InC is employed to determine the duty cycle based on the rule base and the input variables. Prior to constructing the FL, one needs to determine the linguistic terms, membership functions (MF), and rule base. The accuracy relies on the number of linguistic terms. The more linguistic terms used, the more accurate the output will be resulted. However, increasing the number of linguistic terms leads to computational burden. In addition, the parameters of MF and rule base require designers to have some prior knowledge on the P-VCCs to be tracked. Kota $et\ al.$ presented an ANN to track the GMPP under PS. A remarkable tracking time is shown in this method. However, the accuracy of this method strongly depends on the training data. Furthermore, re-collecting data is also needed for other PS conditions.

The MHA is designed to solve an optimization problem which deeply adapts to each problem [32]–[34]. An MHA is very suitable to solve for the GMPP problem under PS conditions as the P-VCCs are generally not known in advance [36].

All MHAs share two common characteristics:

1. They are nature-inspired (based on some principles from biology, ethology, or physics),
2. They make use of stochastic components to escape from local optimal points.

Of the most popular MHA used for MPPT is particle swarm optimization (PSO), due to its easy implementation [37], [38]. However, PSO has the problem of having a long tracking time for large search spaces. In [39], the improved PSO is employed to obtain the GMPP by adding some parameters to determine the new duty cycle based on the power change. However, this mechanism requires to determine some constants based on the duty cycle and maximum power relationship. Researchers have started to seek other MHAs for MPPT. In [40], artificial bee colony (ABC) algorithm has been implemented to obtain the GMPP under PS, and its convergence performance is better than PSO. However, when the number of bees is low, ABC will be trapped in a local maximum power point (LMPP). Ant colony optimization (ACO) used in MPPT was developed by Jiang $et\ al.$ [41]. The performance of ACO is similar to PSO when tested under uniform and shading pattern conditions. The improved differential evolution for achieving GMPP under PS has been proposed by Tey *et al.* [42]. This method provides fast convergence and simple implementation due to the fewer control parameters. However, there is no mechanism to remember the previous movements and locations that the particle have experienced throughout the program. Thus, it tends to be stuck in local maximum. Xin-She Yang and Suash Deb proposed the Cuckoo Search (CS) in 2009 [43], inspired by Cuckoo's brooding behaviors. The algorithm proved to be more effective compared to PSO [44]–[47]. Yet, its convergence rate is slow. A new MHA named Bat Algorithm (BA) proposed by Xin-She Yang is inspired by the echolocation mechanism of bats [48]. The combination of global exploration and local search mechanism allows particles to have less oscillations and good dynamic behavior before reaching the GMPP. The implementation of BA for MPPT to reach GMPP under PS has been reported in [49]–[51]. It is confirmed that BA shows superiority compared to PSO and P&O for MPPT performance [50], [51]. However, the drawback of BA is that under some circumstances, it can be easily trapped in a LMPP, which can reduce the output power of the PV system. Thus, the main contribution of this paper is to improve the performance of the original BA method by enhancing the tracking efficiency and tracking time for MPPT. The proposed modified bat algorithm (MBA) combines the abandonment mechanism from CS with BA. Both simulation and experimental results confirm that the proposed method is able to significantly improve the convergence time and accuracy compared to the original BA. The structure of this paper is as follows. The next section will briefly introduce the principles of BA. The MBA method will be presented in the third section. The simulation results and parameters selections will be elaborated in the fourth section. The fifth section presents the experimental results. Finally, the conclusion is provided in the sixth section.

II. OVERVIEW OF BAT ALGORITHM

Unlike other mammals, bats do not rely on vision. Instead, they use echolocation to detect the environment to avoid

This work is licensed under a Creative Commons Attribution 4.0 License. For more information, see https://creativecommons.org/licenses/by/4.0/.

This article has been accepted for publication in a future issue of this journal, but has not been fully edited. Content may change prior to final publication. Citation information: DOI 10.1109/ACCESS.2020.2993361, IEEE Access

obstacles and catch prey. The operation of echolocation is that the bat first emits a pulse with the appropriate loudness and receives the feedback signals to detect the prey. When the prey gets closer, the bat will increase the pulse volumes and gradually reduce the loudness of the pulse. Hence, bats can detect target distance and even use echolocation to distinguish between obstacles and preys.

The BA proposed by Xin-She Yang in 2010 is inspired by the bat echolocation mechanism. The following rules are defined for the idealized bat algorithm and retain its biological characteristics:

- All bats know the difference between obstacles and preys, via the mechanism of echolocation.
- The bats fly at position X_i at speed V_i, and they adjust the pulse emissivity r_i in the range of [0, 1] according to the degree of proximity to the prey and automatically adjust the frequency of the pulse.
- As the number of iterations increases, the loudness emitted by the bat will gradually decrease from the initial loudness A_0 to minimum A_{min}.

From the above rules, pulse frequency of i th bat, f_i is defined as

$$f_i = f_{min} + (f_{max} - f_{min})\sigma, \tag{1}$$

where f_{min} and f_{max} refer to the minimum and maximum frequencies, respectively, and σ is a random number in the range between 0 and 1.

The speed V_i for the ith bat is expressed as (2).

$$V_i^k = V_i^{k-1} + (X_i^{k-1} - X_{best})f_i, \tag{2}$$

where k is the iteration number, X_{best} is the current global optimal value, and X_i^k is the position of i th bat in the k th iteration, and it is updated based on (3) and (4).

$$X_i^k = X_i^{k-1} + V_i^k, \; if \; r_i^k \leq \sigma_1 \tag{3}$$

$$X_i^k = X_{best} + \beta A^{k-1}, \; if \; r_i^k > \sigma_1, \tag{4}$$

where r_i^k is the pulse emissivity of i th bat in the k th iteration, σ_1 is a random number between 0 and 1, β is a random number between -1 and 1, and A^k is the average loudness of all the bats in the k th iteration. When $r_i^k \leq \sigma_1$, it means that the bat is entering global exploration. When $r_i^k > \sigma_1$, it means bats entering the local search. The pulse emissivity and loudness are updated as the number of iteration increases. When the best solution is still better than the current solution and A_i^k is larger than random number σ_2, the loudness decreases and the pulse emissivity increases. When the loudness and pulse emissivity gets updated, it shows that the bat is looking for prey, and getting closer to it. Therefore, the loudness and pulse emissivity of the i th bat in the k th iteration are defined in (5).

$$A_i^k = \alpha A_i^{k-1}, \quad r_i^k = r_i^0[1 - exp(-\gamma k)], \tag{5}$$

where α and γ are constants. The use of α in the BA is similar to the cooling factor of simulated annealing algorithm [52], [53]. The value ranges are defined as $0 < \alpha < 1$ and $\gamma > 0$, respectively. The trend of loudness and pulse emissivity with the increased number of iterations can be expressed as follows:

$$A_i^k \to A_{min}, \quad r_i^k \to r_i^0, \quad as \; k \to \infty \tag{6}$$

According to (3) to (6), several observations can be made. In the early stage, bats will more easily enter global exploration. During this stage, bats will explore in the opposite direction to the current best solution, which is beneficial in terms of jumping out of the local optimal solution. In the later stage, bats will more likely enter the local search. At this time, they will start with the current global best solution, and the search range will gradually converge according to the loudness.

The convergence criterion as defined in (7) is checked to ensure that global maximum point (GMP) is reached:

$$|X_{best} - X_i^k| \leq \varepsilon, i = 1...N, \tag{7}$$

where N is the number of bats and ε is the tolerance value. When the distances between each bat and current best position are less than ε, the convergence condition is reached.

In an MPPT case, the voltage V is the bat position X and the power P is the fitness of bat $f(X)$. The flowchart of BA is shown in Fig. 1

III. THE PROPOSED MODIFIED BAT ALGORITHM

In this proposed method, BA is combined with the abandonment mechanism from CS in order to accelerate the tracking time. Here, a brief review of the CS algorithm is described to have a better understanding about the abandonment mechanism. CS is inspired from its special brooding method. Cuckoos put their eggs in other birds' nests to increase their hatching rates. However, the cuckoo's eggs can be found by the host bird and these eggs will be destroyed or abandoned. Three idealized characteristic rules for implementing CS are stated as follows:

- Each cuckoo lays an egg and puts it in a randomly selected nest.
- Eggs with high quality will carry over to the next iteration.
- There are a fixed number of host nests in the ecosystem and the probability of alien eggs discovered by the host bird is $P_a \in [0, 1]$.

In case the host bird finds the alien eggs, the nest will be destroyed or abandoned. The host bird then builds a new nest in another place. Note that this can be approximated by replacing a fraction (P_a) of N nests by new solutions.

The abandonment mechanism proposed in CS allows the search to be limited for potentially good candidate solutions. This can speed up the convergence. To improve the convergence speed of the BA, we proposed to infuse the abandonment concept in the BA. The abandonment mechanism is executed immediately after all the particles of BA have been updated via (1) - (5). In the abandonment mechanism,

This work is licensed under a Creative Commons Attribution 4.0 License. For more information, see https://creativecommons.org/licenses/by/4.0/.

This article has been accepted for publication in a future issue of this journal, but has not been fully edited. Content may change prior to final publication. Citation information: DOI 10.1109/ACCESS.2020.2993361, IEEE Access

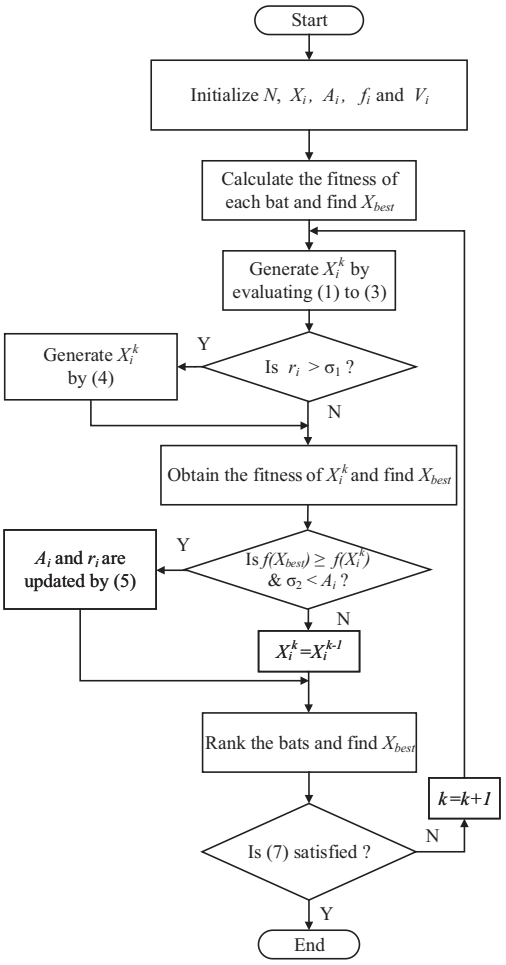

FIGURE 1. The BA flowchart

first, the order of X_i are sorted in the ascending order. Then a number of N_r ($N_r = P_a \times N$) particles are abandoned. To replenish the same number of particles, we first calculate the distance between the global best position X_{best} and the abandoned bat position X_{ai}, $\triangle X_{ai}$, which is defined in (8)

$$\triangle X_{ai} = |X_{best} - X_{ai}| \tag{8}$$

The value of $\triangle X_{ai}$ will be compared with a tolerance value, ε_1. If $\triangle X_{ai}$ is equal to or smaller than ε_1, it implies that X_{ai} is very close to X_{best}. Hence, the replenishing particle, $X_{i,new}$ is set to X_{best}. On the other hand, if $\triangle X_{ai}$ is larger than ε_1, it implies that X_{ai} is far away from X_{best}. Hence, we proposed to set the replenishing particles to have the form of (9)

$$X_{i,new} = X_{best} \pm \triangle S_i \tag{9}$$

$\triangle S_i$ is defined in (10).

$$\triangle S_i = \triangle X_{ai} \cdot N_c \cdot \sigma_3, \tag{10}$$

where σ_3 is the random number in the range between 0 and 1 and N_c is a cooling factor, whose formula is defined as (11).

$$N_c = \frac{1}{k} \tag{11}$$

To determine whether $\triangle S_i$ should be added to or subtracted from X_{best}, the following criteria are evaluated. Assume that X_{ib} represents the best solution of the current iteration. If $X_{best} > X_{ib}$, it means X_{ib} is at the left side of X_{best}. Hence, the replenishing particle, $X_{i,new}$ is set as (12)

$$X_{i,new} = X_{best} - \triangle S_i \tag{12}$$

to explore the left side of X_{best}, as shown in Fig. 3.

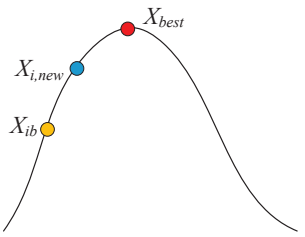

FIGURE 2. The condition of $X_{best} > X_{ib}$

Fig. 4 shows how the search space evolves in this situation. By eliminating X_{ai} in Fig. 4(a), and placing the replenishing particle $X_{i,new}$ according to (12), all the particles are constrained at the left subspace, which can potentially speed up the convergence time. On the other hand, when $X_{best} \leq X_{ib}$, it means X_{ib} is at the right side of X_{best}. Therefore, $X_{i,new}$ is set as (13) to explore the right side of X_{best}, as shown in

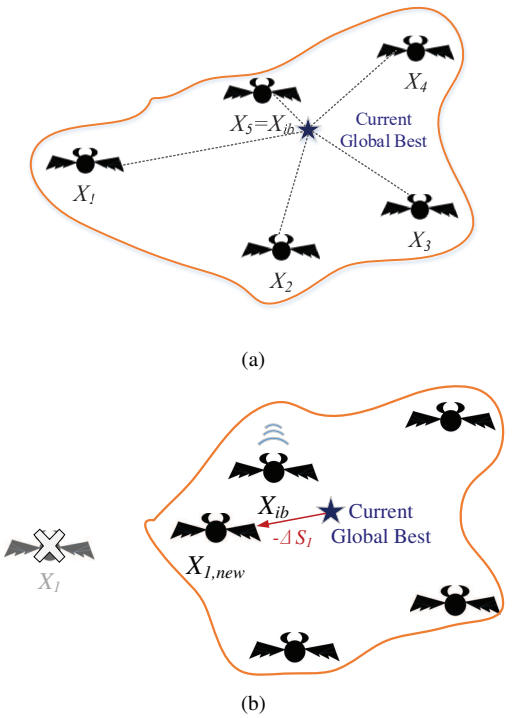

FIGURE 3. Positions of bats when $X_{best} > X_{ib}$: (a) after sorting by fitness, (b) after abandonment mechanism

This work is licensed under a Creative Commons Attribution 4.0 License. For more information, see https://creativecommons.org/licenses/by/4.0/.

This article has been accepted for publication in a future issue of this journal, but has not been fully edited. Content may change prior to final publication. Citation information: DOI 10.1109/ACCESS.2020.2993361, IEEE Access

Fig. 5.

$$X_{i,new} = X_{best} + \triangle S_i \tag{13}$$

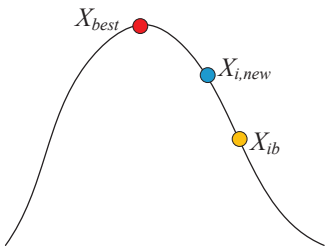

FIGURE 4. The condition of $X_{best} \leq X_{ib}$

Fig. 6 shows how the search space evolves in this situation. By eliminating X_{ai} in Fig. 6(a) and placing the replenishing particle $X_{i,new}$ according to (13), all the particles are constrained at the right subspace.

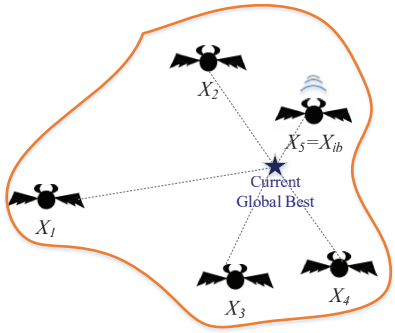

(a)

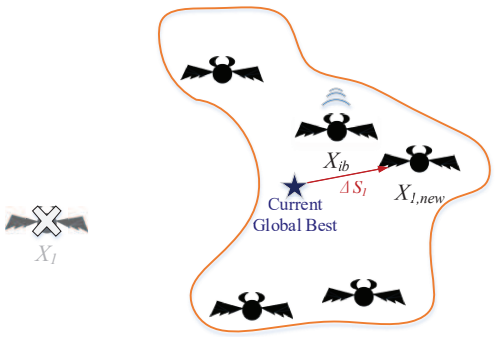

(b)

FIGURE 5. Positions of bats when $X_{best} \leq X_{ib}$: (a) after sorting by fitness, (b) after abandonment mechanism

The updated position $X_{i,new}$ is summarized in Table 1 and the flowchart of MBA is shown in Fig. 7.

IV. SIMULATION RESULTS

Firstly, the proposed method is evaluated through Matlab simulation. Three P-VCCs with different GMPPs are generated to validate the proposed method, and they are displayed in Fig. 8. The number of bats (or "particles") is chosen to be five. Since the converter only has one control parameter (i.e. the duty cycle) to be varied, these five bats need to be executed sequentially for the applications of MPPT. For a fair comparison, all the initial voltage values of BA and MBA are set at 90%, 80%, 70%, 60% and 50% of the open circuit voltage (215 V), respectively. Each waveform runs 1000 times. The parameter selections of BA and MBA are chosen by the results of the average values.

TABLE 1. Conditions for updating $X_{i,new}$

Condition		$X_{i,new}$ Value
$\triangle X_i \leq \varepsilon_1$		X_{best}
$\triangle X_{ai} > \varepsilon 1$	$X_{best} > X_{ib}$	$X_{best} - \triangle S_i$
	$X_{best} \leq X_{ib}$	$X_{best} + \triangle S_i$

BA has two parameters which are α and γ required to be selected. These parameters will affect the convergence time and accuracy. The selection of the parameter is prioritized based on the accuracy. Therefore, the parameters with higher accuracy will be selected to ensure the algorithm can track GMPP efficiently. According to the above rules, through the extensive simulations, the parameter values for α and γ are set to be 0.9 and 0.1, respectively. α is the cooling factor of loudness, which is defined in (5). When α is larger, it means that the loudness will decrease slowly, and vice versa. Several values of α from 0.5 to 0.9 within an interval step of 0.1 have been evaluated. The results are shown in Table 2. According to the accuracy performance, $\alpha = 0.9$ is the best option.

TABLE 2. BA tracking results with various α value

α	Accuracy	Time
0.5	98.43%	5s
0.6	98.55%	4.9s
0.7	98.70%	4.9s
0.8	98.92%	5.1s
0.9 *	99.31%	5.9s

γ adjusts the pulse emissivity of each bat, which determines the frequency of entering the local search. When γ increases, it means the probability of bats moving from global exploration to local search will increase. The results for different values of γ are shown in Table 3. Accordingly, $\gamma = 0.1$ is selected for the best performance.

In MBA, the constants, α and γ are set to be the same as BA. Nevertheless, there is a parameter in MBA, called abandonment number, N_r needs to be set. N_r defines how many bats will be abandoned and created. Several values of P_a from 20% to 100% within an interval step of 20% have

This work is licensed under a Creative Commons Attribution 4.0 License. For more information, see https://creativecommons.org/licenses/by/4.0/.

This article has been accepted for publication in a future issue of this journal, but has not been fully edited. Content may change prior to final publication. Citation information: DOI 10.1109/ACCESS.2020.2993361, IEEE Access

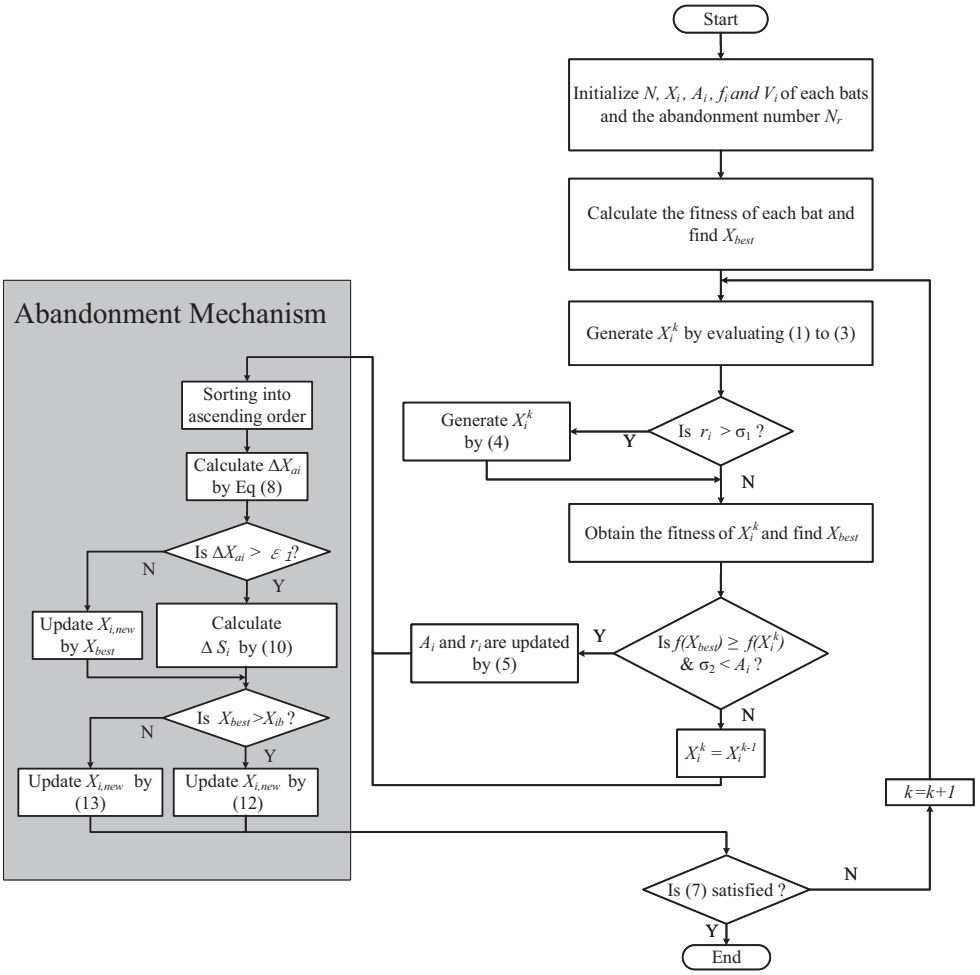

FIGURE 6. The MBA flowchart

TABLE 3. BA tracking result with various γ values

γ	Accuracy	Time
0.1 *	99.31%	5.9s
0.2	98.91%	5.2s
0.3	98.92%	5s
0.4	98.95%	4.8s
0.5	98.95%	4.8s

TABLE 4. MBA tracking result with various N_r values

P_a (%)	$N_r(N \times P_a)$	Accuracy	Time
20	1	99.71%	5.2s
40	2	99.79%	5s
60	3	99.77%	4.6s
80 *	4	99.80%	4.4s
100	5	99.78%	4.4s

been evaluated. The results are shown in Table 4. According to the accuracy performance, $P_a = 80\%$ ($N_r = 4$) is the best option.

Table 5 lists the tracking accuracy and time for each P-VCCs.As indicated in the table, the average accuracy of the MBA is above 99.7% for all the P-VCCs, implying that MBA can successfully track the GMPP, regardless the shapes of P-VCCs. On the other hand, there are some cases that the BA fails to track the GMPP. For example, for curve 2, the tracking efficiency for BA is 97.82%. This can be seen from Fig. 9, showing the distribution histogram of the tracking efficiencies of BA for curve 2. More than 50% of the simulation instances have tracking efficiencies range between 95% and 98%, leading to lower efficiency, compared to MBA. Moreover, the standard deviations of MBA are, on average, smaller than those of the BA, showing the strong

This work is licensed under a Creative Commons Attribution 4.0 License. For more information, see https://creativecommons.org/licenses/by/4.0/.

This article has been accepted for publication in a future issue of this journal, but has not been fully edited. Content may change prior to final publication. Citation information: DOI 10.1109/ACCESS.2020.2993361, IEEE Access

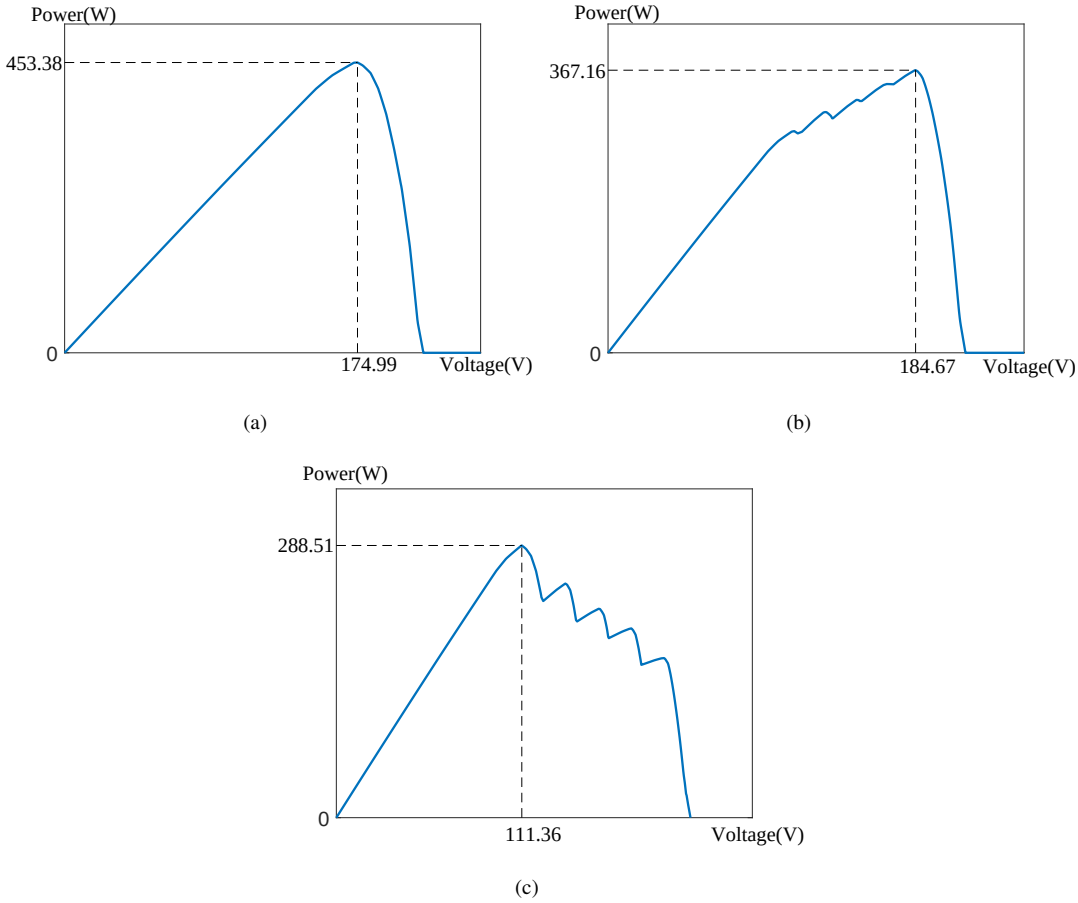

FIGURE 7. The P-VCCs for validation: (a) Curve 1, (b) Curve 2, (c) Curve 3

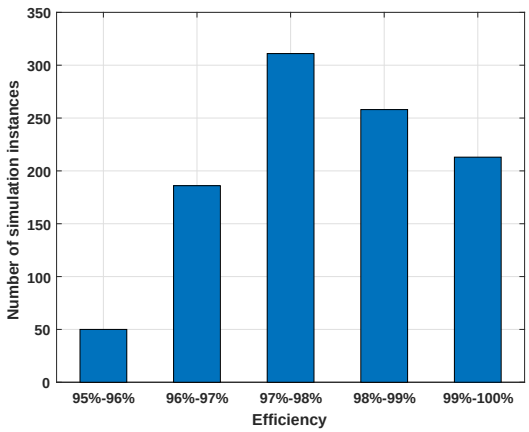

FIGURE 8. The distribution histogram of tracking efficiency of BA for curve 2

consistency of the results for the proposed method. Finally, in terms of the tracking time, the MBA on average saves about 2 (35.7%) seconds when compared to the BA.

V. EXPERIMENTAL VALIDATION

The schematic of the experimental validation is shown in Fig. 10. The DC-DC converter is an interleaved boost converter that can reduce the ripple currents and increase efficiency and reliability. The MPPT algorithms are implemented in a 32-bit digital signal processor (TMS320F28035) from Texas Instruments. The maximum input voltage is 215 V, and the load voltage is maintained at 450 V. The load is a resistive load and its voltage is regulated by a voltage source (Chroma programmable dc power supply 620120P-600-8).

Fig. 11 shows the actual hardware, including DSP, DC-DC converter, loads, oscilloscope, power supply for DSP, programmable DC power supply, and standalone terrestrial solar array photovoltaic emulator (ETS600X8C-PVF).

A. STATIC CASES

The experimental curves, generated from the PV emulator, are the same as those simulated in Matlab. These results are obtained by running the experiments multiple times (more than 20 times). In addition, to compare with BA, the proposed model is also evaluated against two other states-of-the-art MPPT algorithms, and they are PSO and Grey Wolf Optimization (GWO) algorithms. Figs. 12 to 14 show the typical

This work is licensed under a Creative Commons Attribution 4.0 License. For more information, see https://creativecommons.org/licenses/by/4.0/.

This article has been accepted for publication in a future issue of this journal, but has not been fully edited. Content may change prior to final publication. Citation information: DOI 10.1109/ACCESS.2020.2993361, IEEE Access

TABLE 5. Comparison of tracking efficiencies and times for BA and MBA (Simulation)

Curve	Curve			Overall
	No.1	No.2	No.3	
Tracking Efficiency				
BA	99.70±0.08	97.82±1.11	99.81±0.35	99.71±0.51
MBA	99.71±0.09	99.76±0.54	99.83±0.34	99.77±0.32
Tracking Time				
BA	5.7±1	5.8 ±1.4	5.5±1	5.6±1.13
MBA	3.5±0.9	3.2±0.9	4±0.8	3.6±0.87

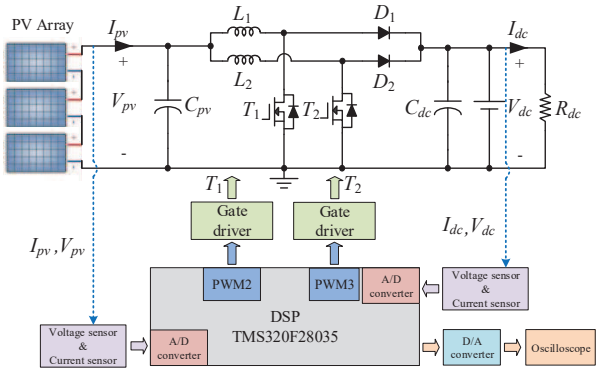

FIGURE 9. The schematic of hardware configuration

tracking trajectories of the BA, MBA, PSO, and GWO. Note that since the number of the particles used is 5, generally, one iteration comprises of five voltage changes. To ensure that the response time of the PV emulator is faster than the controller response, the particle is updated every 100 ms. Hence, one iteration takes 500 ms. As shown in Fig.12, it takes 12 iterations for the BA to attain GMPP for curve 1, while it takes slightly more than seven iterations for the MBA to converge. On the other hand, it requires 12 and 13 iterations for GWO and PSO, respectively to attain the GMPP. Similarly, Figs. 13 and 14 show that the MBA can get to the GMPP much faster than the BA, PSO, and GWO for curves 2 and 3. Moreover, as Fig. 12-14 show, all the particles are initialized at 90%, 80%, 70%, 60%, and 50% of the open-circuit voltage. Thus, in the first iteration, the voltage profiles are the same for all the methods. Nevertheless, the voltage trajectories are different from these algorithms after the first iteration due to different ways of searching for the GMPP. The MBA exhibits the least voltage variances among the other methods. This is because the MBA incorporates the abandonment mechanism of CS into the BA, allowing the search to be limited to the potentially good candidate solutions. For instance, in Fig. 12, one can see that after the fifth iteration, all the five particles are close to each other and

TABLE 6. Comparison of tracking efficiencies and times for BA, MBA, PSO, and GWO (Experiment)

Method	Curve			Overall
	No.1	No.2	No.3	
Tracking Accuracy				
BA	99.7±0.08	99.72±1.11	99.81±0.35	99.74±0.51
MBA	99.81±0.1	99.92±0.54	99.83±0.34	99.85±0.35
PSO	99.2±2	98.73±0.3	98.52±0.5	98.81±0.81
GWO	99.8±0.3	99.72±0.8	99.82±0.07	99.78±0.1
Tracking Time				
BA	5.9±1.5	5.6±1.4	5.4±0.1	5.5±1.2
MBA	3.4±0.9	3±0.9	3.7±0.1.3	3.6±01.1
PSO	6.7±1.8	6.8±0.5	6.5±2	6.6±1.4
GWO	5.6±1.5	6 ±1.1	5.8±1	5.8±1.2

This work is licensed under a Creative Commons Attribution 4.0 License. For more information, see https://creativecommons.org/licenses/by/4.0/.

This article has been accepted for publication in a future issue of this journal, but has not been fully edited. Content may change prior to final publication. Citation information: DOI 10.1109/ACCESS.2020.2993361, IEEE Access

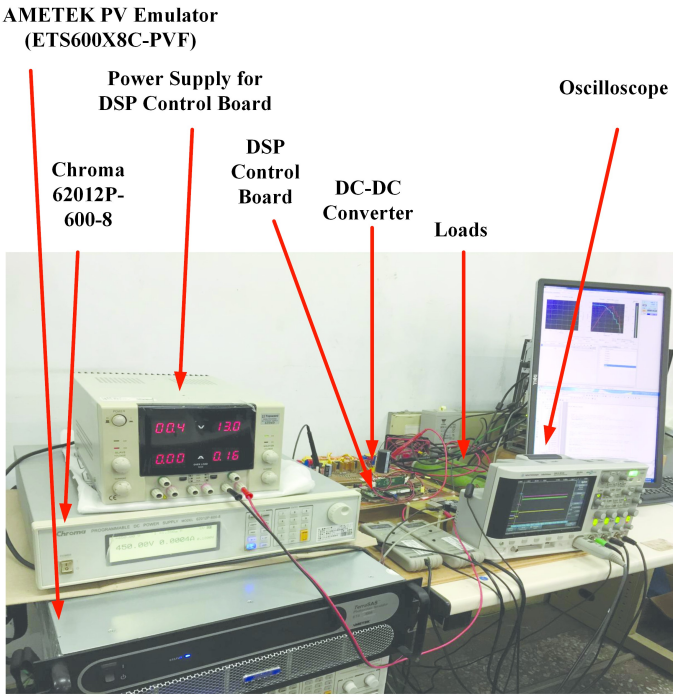

FIGURE 10. The actual hardware setup

only take another two iterations to converge to the GMPP. On the other hand, all the other three algorithms exhibit high voltage fluctuations. In particular, the GWO has the highest voltage variations. In fact, the highest voltage variations for all four methods are 38.76 V for MBA, 119.1 V for BA, 80.4 V for PSO, and 128.47 V for GWO. The reason why GWO exhibits highest voltage variations is that the GWO allows the particles to search in a wider search space for the first few iterations. Then, the GWO will explore a smaller region in much later iterations to track GMPP. From Figs. 12-14, we can see that BA generally perform better rather than PSO, confirming the findings in the literature. Nevertheless, BA has longer tracking time, and higher variations, as compared to the MBA.

The tracking efficiency and tracking time of all MPPT algorithms are summarized in Table 6. Generally, the proposed method yields better results compared to BA, PSO, and GWO, achieving an average accuracy of 99.85% with 0.35 standard deviation. On average, the tracking time for the proposed method is about 3.6 seconds, while the other algorithms cannot reach values under 5 seconds. Compared to the BA, an improvement of 1.9 seconds (34.5%) can be attained by using the proposed method. It is worth noting that, generally, there is a trade-off between tracking time and efficiency for an MPPT algorithm. That is, high tracking accuracy is usually achieved at the expense of longer tracking time. The proposed method, combined with the abandonment mechanism of cuckoo search, can improve both the tracking time and efficiency, demonstrating the superiority of the proposed method.

The experimental results generally are in agreement with the simulation results, showing the proposed MBA has a better performance compared to another algorithm. Some slight discrepancies between the simulation and experiment results are due to the following:

1. The converter is assumed to be ideal in the simulation whereas the actual converter has switching and conduction losses.
2. Due to the hardware constraints and thermal limitations, the number of experiment conducted is much smaller than the number of simulations.

Finally, Table 7 lists the computational costs required by each MPPT algorithm during the first 10 seconds. Such a period is chosen, since all algorithm successfully converges at 10 seconds. It can be clearly seen that the proposed method, on average, requires the least computational costs compared to other algorithm.

B. DYNAMIC CASES

The actual environmental conditions are ever-changing, and the changes of irradiance and temperature will affect P-VCC. Continuous variations of P-VCCs will be generated in the PV emulator to test the dynamic tracking capability of the proposed MPPT algorithm. In this study, the starting power level is 453.38 W while the ending power level is 288.51 W in continuous dynamic tracking. The changing sequence of P-VCCs are shown in Fig. 15, and the shading patterns and the irradiance levels are changed every 11 seconds. The choice of 11 seconds is due to the tracking time of the BA in the worst case is about 5.5 seconds. Therefore, the changing time is set to 11 seconds, which is two times of 5.5 seconds. This is to ensure that there is enough time for each waveform to settle.

To detect the power variations caused by irradiance or temperature changes, (14) is defined.

$$|P_{pv} - P_{pv,last}| \geq \triangle P, \tag{14}$$

where $P_{pv,last}$ is the power of the previous detection and $\triangle P$ is set to 5% of the maximum power. When the current power P_{pv} differs from the previous power $P_{pv,last}$ is larger than $\triangle P$, it means that power variations have occurred. Therefore, the algorithm will reinitialize and re-track the new GMPP. Note that $\triangle P$ needs to be carefully selected such that it is able to distinguish the fluctuations of the output power caused by the noise of voltage or the irradiance variations.

The efficiency of dynamic tracking η_d is defined as follows:

$$\eta_d = \frac{\sum_i V_{pv,i} \cdot I_{pv,i} \cdot \triangle T_i}{\sum_j GMP_j \cdot \triangle T_j} \times 100\%, \tag{15}$$

where $\triangle T_j$ is the period in which the GMP_j is provided and $\triangle T_i$ is the period in which $V_{pv,i}$ and $I_{pv,i}$ are sampled. The results of dynamic experiments are shown in Figs. 16 and 17. The tracking efficiency for BA and MBA are 94.38% and 96.7%, respectively. Figs.16 and 17 show the dynamic tracking performance of BA and MBA. MBA can enhance the dynamic efficiency by nearly 2.5% due to the following

This work is licensed under a Creative Commons Attribution 4.0 License. For more information, see https://creativecommons.org/licenses/by/4.0/.

This article has been accepted for publication in a future issue of this journal, but has not been fully edited. Content may change prior to final publication. Citation information: DOI 10.1109/ACCESS.2020.2993361, IEEE Access

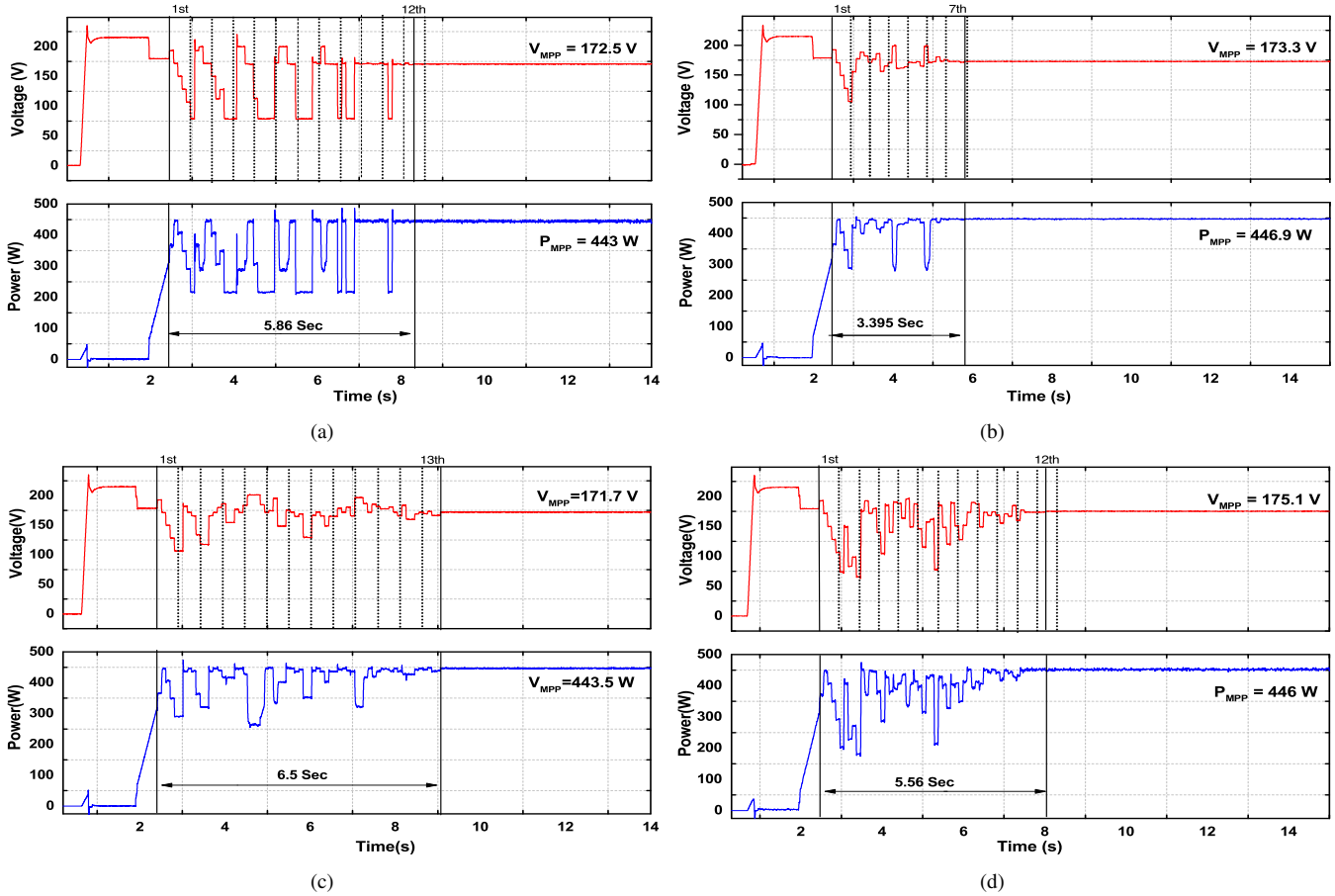

FIGURE 11. The comparison of voltage and power trajectories for P-VCC curve 1: (a) BA, (b) MBA, (c) PSO, and (d) GWO

TABLE 7. Numbers of mathematical operations before the maximum power is achieved

	1						2						3					
	+	×	−	/	e^x	Total	+	×	−	/	e^x	Total	+	×	−	/	e^x	Total
BA	192	60	96	120	12	480	186	55	88	110	11	450	186	55	87	109	11	448
MBA	174	41	67	88	7	377	167	35	61	77	6	347	170	38	64	81	6	359
PSO	991	447	409	502	268	2617	991	447	408	502	268	2617	965	443	397	490	260	2555
GWO	954	945	520	400	0	2820	1005	1003	551	425	0	2984	975	969	533	410	0	2887

reasons. The MBA exhibits much less power and voltage fluctuations, compared with the BA. Moreover, the MBA takes less time to settle to the GMPP whenever a power change is detected. This case study clearly demonstrates that the MBA can effectively track the GMPP with a much shorter convergence time and a smoother profile, leading to higher dynamic efficiency.

VI. CONCLUSION

This paper employs the abandonment mechanism from CS to improve the BA for MPPT of a PV system. By retaining the high-quality solution and abandoning poor solution, the abandonment mechanism added to BA can increase the probability of getting out of the LMPP and decrease the tracking time. The experimental results show that the static tracking accuracies of the proposed method are above 99.80%. Moreover, MBA can enhance the dynamic tracking efficiency by 2.5% and decrease the tracking time by almost 35% compared to BA.

REFERENCES

[1] I. E. A. (IEA), "Modern bioenergy leads the growth of all renewables to 2023, according to latest iea market forecast," 2018. [Online]. Available: https://www.iea.org/newsroom/news/2018/october/modern-bioenergy-leads-the-growth-of-all-renewables-to-2023-accord-.ing-to-latest-.html

[2] F. Nadeem, S. M. S. Hussain, P. K. Tiwari, A. K. Goswami, and T. S. Ustun, "Comparative review of energy storage systems, their roles, and impacts on future power systems," IEEE Access, vol. 7, pp. 4555–4585, 2019.

[3] D. Koraki and K. Strunz, "Wind and solar power integration in electricity markets and distribution networks through service-centric virtual power plants," IEEE Transactions on Power Systems, vol. 33, no. 1, pp. 473–485, Jan 2018.

[4] I. E. A. (IEA), "The latest trends in energy and emissions in 2018," 2019. [Online]. Available: https://webstore.iea.org/global-energy-co2-status-report-2018

[5] M. A. Ghasemi, A. Ramyar, and H. Iman-Eini, "Mppt method for pv

This work is licensed under a Creative Commons Attribution 4.0 License. For more information, see https://creativecommons.org/licenses/by/4.0/.

This article has been accepted for publication in a future issue of this journal, but has not been fully edited. Content may change prior to final publication. Citation information: DOI 10.1109/ACCESS.2020.2993361, IEEE Access

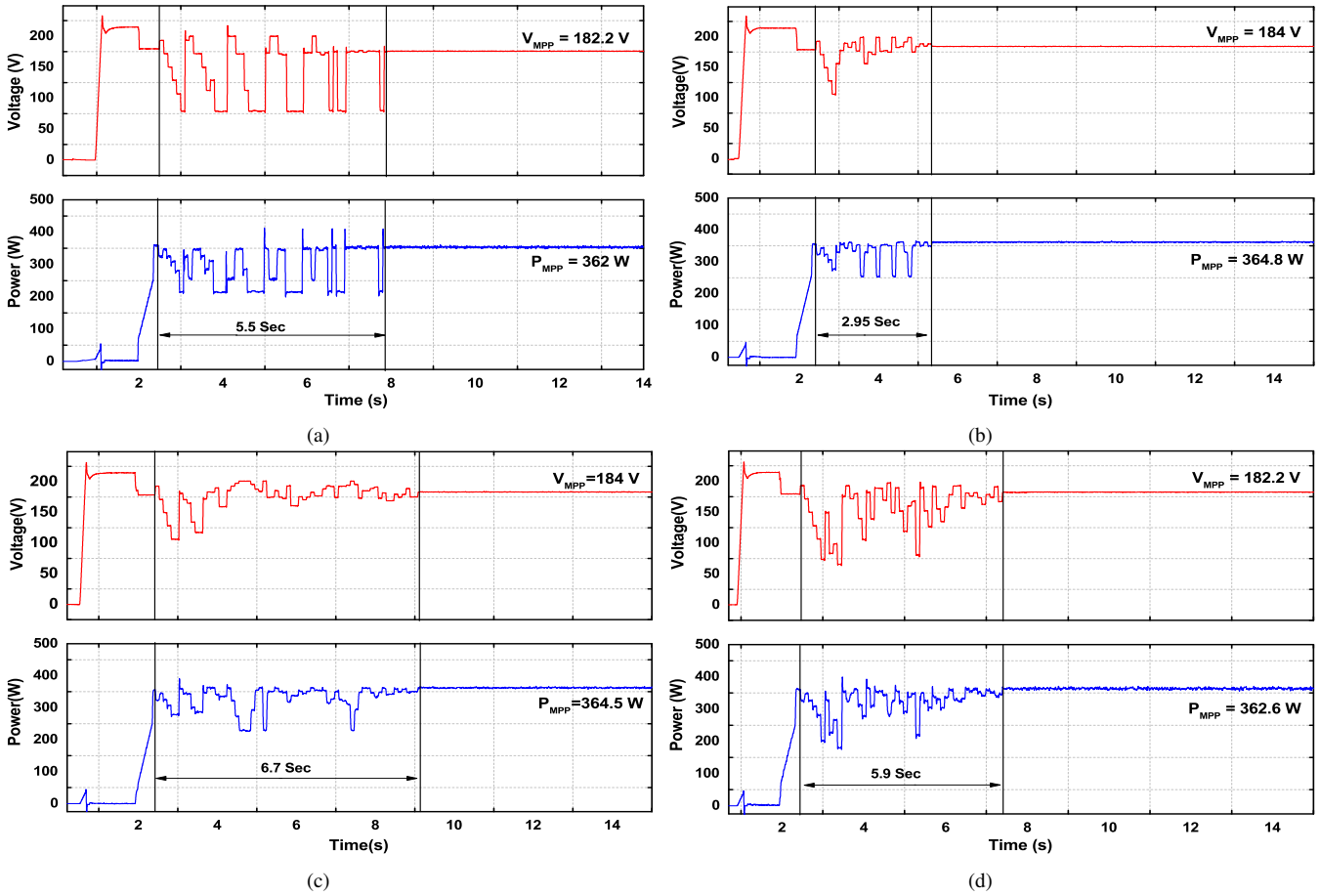

FIGURE 12. The comparison of voltage and power trajectories for P-VCC curve 2: (a) BA, (b) MBA, (c) PSO, and (d) GWO

systems under partially shaded conditions by approximating iâĂŞv curve," IEEE Transactions on Industrial Electronics, vol. 65, no. 5, pp. 3966–3975, May 2018.

[6] M. Malinowski, J. I. Leon, and H. Abu-Rub, "Solar photovoltaic and thermal energy systems: Current technology and future trends," Proceedings of the IEEE, vol. 105, no. 11, pp. 2132–2146, Nov 2017.

[7] H. Li, D. Yang, W. Su, J. LÃij, and X. Yu, "An overall distribution particle swarm optimization mppt algorithm for photovoltaic system under partial shading," IEEE Transactions on Industrial Electronics, vol. 66, no. 1, pp. 265–275, Jan 2019.

[8] A. M. S. Furtado, F. Bradaschia, M. C. Cavalcanti, and L. R. Limongi, "A reduced voltage range global maximum power point tracking algorithm for photovoltaic systems under partial shading conditions," IEEE Transactions on Industrial Electronics, vol. 65, no. 4, pp. 3252–3262, April 2018.

[9] A. Chakri, R. Khelif, M. Benouaret, and X.-S. Yang, "New directional bat algorithm for continuous optimization problems," Expert Systems with Applications, vol. 69, pp. 159 – 175, 2017. [Online]. Available: http://www.sciencedirect.com/science/article/pii/S0957417416305905

[10] O. BingÃűl and B. ÃŰzkaya, "Analysis and comparison of different pv array configurations under partial shading conditions," Solar Energy, vol. 160, pp. 336 – 343, 2018. [Online]. Available: http://www.sciencedirect.com/science/article/pii/S0038092X17310769

[11] P. Guerriero, P. Tricoli, and S. Daliento, "A bypass circuit for avoiding the hot spot in pv modules," Solar Energy, vol. 181, pp. 430 – 438, 2019. [Online]. Available: http://www.sciencedirect.com/science/article/pii/S0038092X19301355

[12] S. Daliento, F. D. Napoli, P. Guerriero, and V. dâĂŹAlessandro, "A modified bypass circuit for improved hot spot reliability of solar panels subject to partial shading," Solar Energy, vol. 134, pp. 211 – 218, 2016. [Online]. Available: http://www.sciencedirect.com/science/article/pii/S0038092X16300810

[13] M. A. Ghasemi, H. Mohammadian Foroushani, and M. Parniani, "Partial shading detection and smooth maximum power point tracking of pv arrays under psc," IEEE Transactions on Power Electronics, vol. 31, no. 9, pp. 6281–6292, Sep. 2016.

[14] H. Li, D. Yang, W. Su, J. LÃij, and X. Yu, "An overall distribution particle swarm optimization mppt algorithm for photovoltaic system under partial shading," IEEE Transactions on Industrial Electronics, vol. 66, no. 1, pp. 265–275, Jan 2019.

[15] M. Seyedmahmoudian, R. Rahmani, S. Mekhilef, A. Maung Than Oo, A. Stojcevski, T. K. Soon, and A. S. Ghandhari, "Simulation and hardware implementation of new maximum power point tracking technique for partially shaded pv system using hybrid depso method," IEEE Transactions on Sustainable Energy, vol. 6, no. 3, pp. 850–862, July 2015.

[16] J. Prasanth Ram and N. Rajasekar, "A novel flower pollination based global maximum power point method for solar maximum power point tracking," IEEE Transactions on Power Electronics, vol. 32, no. 11, pp. 8486–8499, Nov 2017.

[17] M. Killi and S. Samanta, "Modified perturb and observe mppt algorithm for drift avoidance in photovoltaic systems," IEEE Transactions on Industrial Electronics, vol. 62, no. 9, pp. 5549–5559, Sep. 2015.

[18] A. K. Abdelsalam, A. M. Massoud, S. Ahmed, and P. N. Enjeti, "High-performance adaptive perturb and observe mppt technique for photovoltaic-based microgrids," IEEE Transactions on Power Electronics, vol. 26, no. 4, pp. 1010–1021, April 2011.

[19] S. K. Kollimalla and M. K. Mishra, "A novel adaptive p o mppt algorithm considering sudden changes in the irradiance," IEEE Transactions on Energy Conversion, vol. 29, no. 3, pp. 602–610, Sep. 2014.

[20] W. Zhu, L. Shang, P. Li, and H. Guo, "Modified hill climbing mppt algorithm with reduced steady-state oscillation and improved tracking efficiency," The Journal of Engineering, vol. 2018, no. 17, pp. 1878–1883, 2018.

[21] K. S. Tey and S. Mekhilef, "Modified incremental conductance algorithm for photovoltaic system under partial shading conditions and load vari-

This work is licensed under a Creative Commons Attribution 4.0 License. For more information, see https://creativecommons.org/licenses/by/4.0/.

This article has been accepted for publication in a future issue of this journal, but has not been fully edited. Content may change prior to final publication. Citation information: DOI 10.1109/ACCESS.2020.2993361, IEEE Access

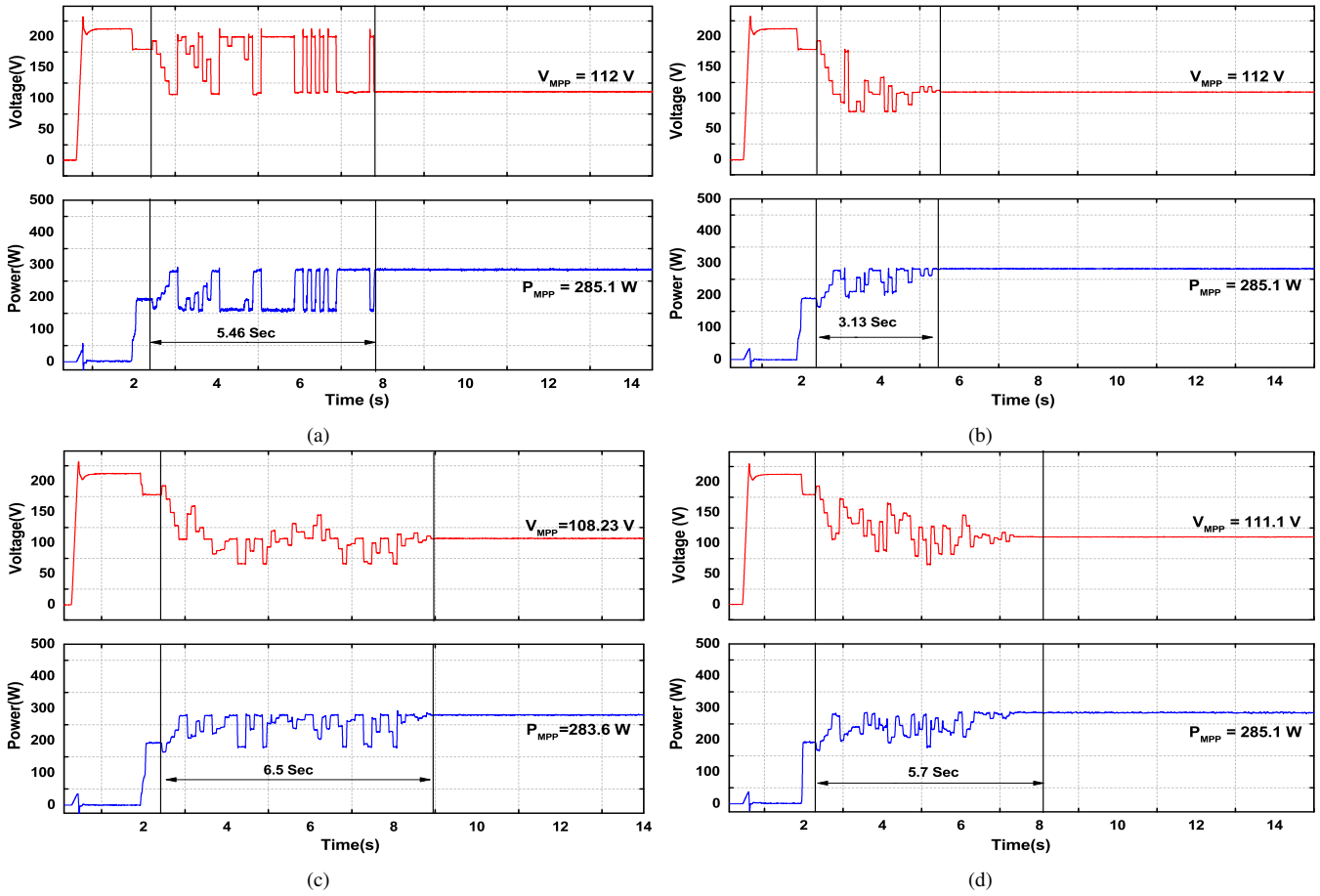

FIGURE 13. The comparison of voltage and power trajectories for P-VCC curve 3: (a) BA, (b) MBA, (c) PSO, and (d) GWO

ation," IEEE Transactions on Industrial Electronics, vol. 61, no. 10, pp. 5384–5392, Oct 2014.

[22] A. Safari and S. Mekhilef, "Simulation and hardware implementation of incremental conductance mppt with direct control method using cuk converter," IEEE Transactions on Industrial Electronics, vol. 58, no. 4, pp. 1154–1161, April 2011.

[23] S. K. Kollimalla and M. K. Mishra, "Variable perturbation size adaptive p o mppt algorithm for sudden changes in irradiance," IEEE Transactions on Sustainable Energy, vol. 5, no. 3, pp. 718–728, July 2014.

[24] L. Piegari and R. Rizzo, "Adaptive perturb and observe algorithm for photovoltaic maximum power point tracking," IET Renewable Power Generation, vol. 4, no. 4, pp. 317–328, July 2010.

[25] T. K. Soon and S. Mekhilef, "A fast-converging mppt technique for photovoltaic system under fast-varying solar irradiation and load resistance," IEEE Transactions on Industrial Informatics, vol. 11, no. 1, pp. 176–186, Feb 2015.

[26] B. N. Alajmi, K. H. Ahmed, S. J. Finney, and B. W. Williams, "Fuzzy-logic-control approach of a modified hill-climbing method for maximum power point in microgrid standalone photovoltaic system," IEEE Transactions on Power Electronics, vol. 26, no. 4, pp. 1022–1030, April 2011.

[27] C. Larbes, S. A. Cheikh, T. Obeidi, and A. Zerguerras, "Genetic algorithms optimized fuzzy logic control for the maximum power point tracking in photovoltaic system," Renewable Energy, vol. 34, no. 10, pp. 2093 – 2100, 2009. [Online]. Available: http://www.sciencedirect.com/science/article/pii/S0960148109000135

[28] A. Messai, A. Mellit, A. Guessoum, and S. Kalogirou, "Maximum power point tracking using a ga optimized fuzzy logic controller and its fpga implementation," Solar Energy, vol. 85, no. 2, pp. 265 – 277, 2011. [Online]. Available: http://www.sciencedirect.com/science/article/pii/S0038092X10003695

[29] V. R. Kota and M. N. Bhukya, "A novel global mpp tracking scheme based on shading pattern identification using artificial neural networks for photovoltaic power generation during partial shaded condition," IET Renewable Power Generation, vol. 13, no. 10, pp. 1647–1659, 2019.

[30] W. Lin, C. Hong, and C. Chen, "Neural-network-based mppt control of a stand-alone hybrid power generation system," IEEE Transactions on Power Electronics, vol. 26, no. 12, pp. 3571–3581, Dec 2011.

[31] L. M. Elobaid, A. K. Abdelsalam, and E. E. Zakzouk, "Artificial neural network-based photovoltaic maximum power point tracking techniques: a survey," IET Renewable Power Generation, vol. 9, no. 8, pp. 1043–1063, 2015.

[32] P. Savsani, R. L. Jhala, and V. J. Savsani, "Comparative study of different metaheuristics for the trajectory planning of a robotic arm," IEEE Systems Journal, vol. 10, no. 2, pp. 697–708, June 2016.

[33] E.-G. Talbi, Metaheuristics: From Design to Implementation. Wiley Publishing, 2009.

[34] X.-S. Yang, "Metaheuristic optimization: Algorithm analysis and open problems," in Experimental Algorithms, P. M. Pardalos and S. Rebennack, Eds. Berlin, Heidelberg: Springer Berlin Heidelberg, 2011, pp. 21–32.

[35] T. Radjai, L. Rahmani, S. Mekhilef, and J. P. Gaubert, "Implementation of a modified incremental conductance mppt algorithm with direct control based on a fuzzy duty cycle change estimator using dspace," Solar Energy, vol. 110, pp. 325 – 337, 2014. [Online]. Available: http://www.sciencedirect.com/science/article/pii/S0038092X14004447

[36] W. He, X. Luo, O. Kiselychnyk, J. Wang, and M. H. Shaheed, "Maximum power point tracking (mppt) control of pressure retarded osmosis (pro) salinity power plant: Development and comparison of different techniques," Desalination, vol. 389, pp. 187 – 196, 2016, pressure Retarded Osmosis. [Online]. Available: http://www.sciencedirect.com/science/article/pii/S0011916416300236

[37] H. Li, D. Yang, W. Su, J. LÃij, and X. Yu, "An overall distribution particle swarm optimization mppt algorithm for photovoltaic system under partial

This work is licensed under a Creative Commons Attribution 4.0 License. For more information, see https://creativecommons.org/licenses/by/4.0/.

This article has been accepted for publication in a future issue of this journal, but has not been fully edited. Content may change prior to final publication. Citation information: DOI 10.1109/ACCESS.2020.2993361, IEEE Access

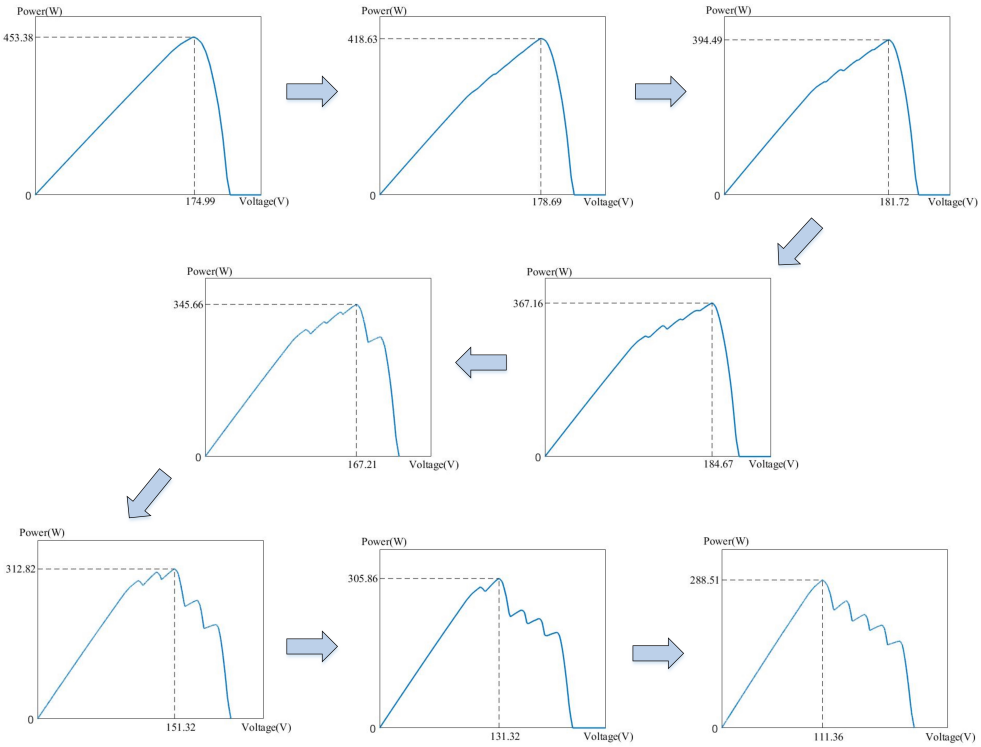

FIGURE 14. Dynamic variations of P-VCCs under PS conditions

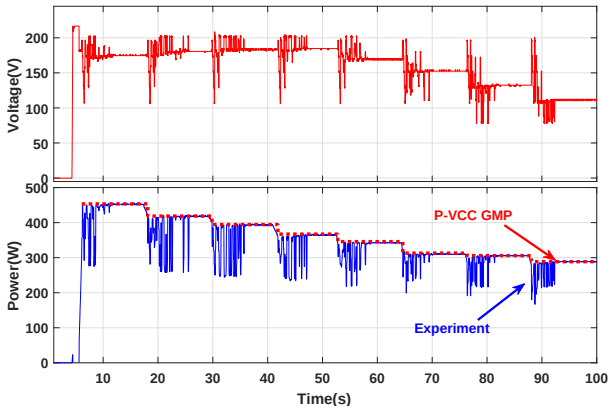

FIGURE 15. The voltage and power response using BA under dynamic case

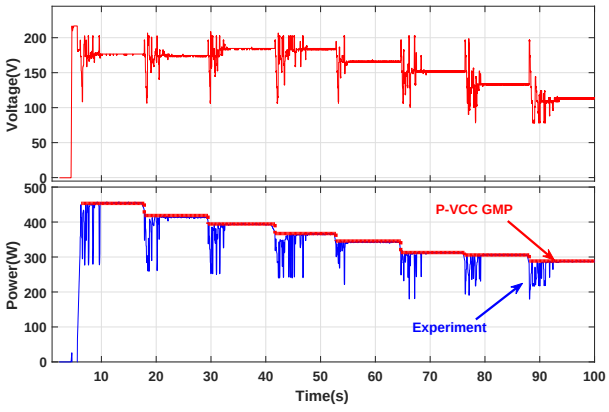

FIGURE 16. The voltage and power response using MBA under dynamic case

shading," IEEE Transactions on Industrial Electronics, vol. 66, no. 1, pp. 265–275, Jan 2019.

[38] J. Zhang, M. Cui, and Y. He, "Robustness and adaptability analysis for equivalent model of doubly fed induction generator wind farm using measured data," Applied Energy, vol. 261, p. 114362, 2020. [Online]. Available: http://www.sciencedirect.com/science/article/pii/S0306261919320495

[39] K. Ishaque, Z. Salam, M. Amjad, and S. Mekhilef, "An improved particle swarm optimization (pso)âĂŞbased mppt for pv with reduced steady-state oscillation," IEEE Transactions on Power Electronics, vol. 27, no. 8, pp. 3627–3638, Aug 2012.

[40] K. Sundareswaran, P. Sankar, P. S. R. Nayak, S. P. Simon, and S. Palani, "Enhanced energy output from a pv system under partial shaded conditions through artificial bee colony," IEEE Transactions on Sustainable Energy, vol. 6, no. 1, pp. 198–209, Jan 2015.

[41] L. L. Jiang and D. L. Maskell, "A uniform implementation scheme for evolutionary optimization algorithms and the experimental implementation of an aco based mppt for pv systems under partial shading," in 2014 IEEE Symposium on Computational Intelligence Applications in Smart Grid (CIASG), Dec 2014, pp. 1–8.

[42] K. S. Tey, S. Mekhilef, M. Seyedmahmoudian, B. Horan, A. T. Oo, and A. Stojcevski, "Improved differential evolution-based mppt algorithm using sepic for pv systems under partial shading conditions and load variation," IEEE Transactions on Industrial Informatics, vol. 14, no. 10, pp. 4322–4333, Oct 2018.

[43] X. Yang and Suash Deb, "Cuckoo search via lÃľvy flights," in 2009 World Congress on Nature Biologically Inspired Computing (NaBIC), Dec 2009, pp. 210–214.

[44] B. Peng, K. Ho, and Y. Liu, "A novel and fast mppt method suitable for both fast changing and partially shaded conditions," IEEE Transactions on Industrial Electronics, vol. 65, no. 4, pp. 3240–3251, April 2018.

[45] M. Kermadi, Z. Salam, J. Ahmed, and E. M. Berkouk, "An effective hybrid

This work is licensed under a Creative Commons Attribution 4.0 License. For more information, see https://creativecommons.org/licenses/by/4.0/.

This article has been accepted for publication in a future issue of this journal, but has not been fully edited. Content may change prior to final publication. Citation information: DOI 10.1109/ACCESS.2020.2993361, IEEE Access

maximum power point tracker of photovoltaic arrays for complex partial shading conditions," IEEE Transactions on Industrial Electronics, vol. 66, no. 9, pp. 6990–7000, Sep. 2019.

[46] J. Ahmed and Z. Salam, "An enhanced adaptive p o mppt for fast and efficient tracking under varying environmental conditions," IEEE Transactions on Sustainable Energy, vol. 9, no. 3, pp. 1487–1496, July 2018.

[47] J. Ahmed and Z. Salam, "A maximum power point tracking (mppt) for pv system using cuckoo search with partial shading capability," Applied Energy, vol. 119, pp. 118 – 130, 2014. [Online]. Available: http://www.sciencedirect.com/science/article/pii/S0306261914000026

[48] X. Yang and A. H. Gandomi, "Bat algorithm: a novel approach for global engineering optimization," Engineering Computations, vol. 29, no. 5, pp. 464–483, 2012. [Online]. Available: https://doi.org/10.1108/02644401211235834

[49] K. S. Tey, S. Mekhilef, and M. Seyedmahmoudian, "Implementation of bat algorithm as maximum power point tracking technique for photovoltaic system under partial shading conditions," in 2018 IEEE Energy Conversion Congress and Exposition (ECCE), Sep. 2018, pp. 2531–2535.

[50] K. Kaced, C. Larbes, N. Ramzan, M. Bounabi, and Z. elabadine Dahmane, "Bat algorithm based maximum power point tracking for photovoltaic system under partial shading conditions," Solar Energy, vol. 158, pp. 490 – 503, 2017. [Online]. Available: http://www.sciencedirect.com/science/article/pii/S0038092X17308599

[51] A. S. Oshaba, E. S. Ali, and S. M. Abd Elazim, "Pi controller design for mppt of photovoltaic system supplying srm via bat search algorithm," Neural Computing and Applications, vol. 28, no. 4, pp. 651–667, Apr 2017. [Online]. Available: https://doi.org/10.1007/s00521-015-2091-9

[52] S. Lyden and M. E. Haque, "A simulated annealing global maximum power point tracking approach for pv modules under partial shading conditions," IEEE Transactions on Power Electronics, vol. 31, no. 6, pp. 4171–4181, June 2016.

[53] Z. Lin, J. Wang, Z. Fang, M. Hu, C. Cai, and J. Zhang, "Accurate maximum power tracking of wireless power transfer system based on simulated annealing algorithm," IEEE Access, vol. 6, pp. 60 881–60 890, 2018.

CHIH YU LIAO received the B.Sc, in electrical engineering from the National Taipei University of Technology and the M.Sc. degree in electrical engineering at National Taiwan University of Science and Technology, Taipei City, Taiwan in 2019.

RAMADHANI KURNIAWAN SUBROTO (M'19) received the B.Eng degree in electrical engineering from Institut Teknologi Sepuluh Nopember, Surabaya, Indonesia in 2012 and the M.Eng and M.Sc degrees from Institut Teknologi Sepuluh Nopember and National Taiwan University of Science and Technology, Taiwan in 2014. He serves as faculty member in Department of Electrical Engineering, Brawijaya University, Malang, Indonesia. He is currently pursuing his Ph.D degree with National Taiwan University of Science and Technology, Taipei City, Taiwan.

IBRAHIM SAIFUL MILLAH received the B.Eng degree in electrical engineering from University of Jember, Jember, Indonesia in 2017. He is currently chasing his Master degree in electrical engineering at National Taiwan University of Science and Technology, Taipei City, Taiwan.

KUO LUNG LIAN (SM'14) received the B.A.Sc.(Hons.), M.A.Sc., and Ph. D. degrees in electrical engineering in 2001, 2003, and 2007, respectively, from the University of Toronto, Toronto, ON, Canada. He was a Visiting Research Scientist with the Central Research Institute of Electric Power Industry, Japan, from October 2007 to January 2009. He is currently an Associate Professor with the National Taiwan University of Science and Technology, Taipei City, Taiwan.

WEI-TZER HUANG (M'04) was born in Taiwan, R.O.C., on August 15, 1971. He received his B.S., M.S. and Ph. D. degrees in electrical engineering from National Taiwan University of Science and Technology, Taipei, Taiwan, the Republic of China, in 1997, 1999 and 2005, respectively. Presently, he is a professor of National Changhua University of Education. His research interests include modeling and simulation of power systems, microgrids modeling and online management, and power electronics.

This work is licensed under a Creative Commons Attribution 4.0 License. For more information, see https://creativecommons.org/licenses/by/4.0/.